Dependence of Dynamic Loss on Critical Current and n-value of HTS Coated Conductors

Dependence of Dynamic Loss on Critical Current and *n*-value of HTS Coated Conductors

Hongye Zhang, Min Yao, Zhenan Jiang, Ying Xin, and Quan Li

***Abstract*—Properties of superconductors, such as critical current and *n*-value, have a significant impact on their loss characteristics. This impact is essential for the design of superconducting devices and their loss reduction, and therefore need to be thoroughly understood. The dependence of AC loss in high temperature superconductors (HTS) on these properties has been well studied. However, it is still unknown how dynamic loss is affected. This paper is to address this unsolved problem and provide comprehensive analyses through both numerical simulation and experimental measurements. In this paper, HTS coated conductors with a wide range of critical currents and *n*-values have been extensively studied. Their dynamic losses and resistance under various conditions have been modelled and compared to available experiment measurements. Results clearly show the dependence of dynamic loss and resistance on critical current and *n*-value. The cases with high current load under strong external magnetic field have been studied as well. All these results show a rapid change of dynamic loss around certain magnetic fields, which we defined to be the "corner field", B_{cor}. This paper clearly demonstrates the dependence of dynamic loss and resistance on critical current and *n*-value, which can be used as a reference for material selection and design optimization.**

***Index Terms*—HTS coated conductor, dynamic loss, dynamic resistance, critical current, *n*-value.**

I. Introduction

DYNAMIC loss and dynamic resistance have aroused widespread concern recently in the domain of high-temperature superconductors (HTS) [1]-[4]. It is generated inside the superconductor carrying direct current (DC) in an alternating magnetic field environment. HTS coated conductors (CCs) are becoming more and more favored because of their growing maturity and ameliorated cost performance with the technological progress, therefore they turn out to be an advantageous alternative to traditional conductors in power industry, such as rotating machines [5]-[10].

This work was supported by the joint scholarship from the University of Edinburgh and China Scholarship Council under grant [2018] 3101. (*Corresponding author: Quan Li, Quan.Li@ed.ac.uk.*)

H.-Y. Zhang, Q. Li, and M. Yao are with the School of Engineering, University of Edinburgh, Edinburgh, EH9 3JL, U.K. (e-mail: Hongye.Zhang@ed.ac.uk; Min.Yao@ed.ac.uk, Quan.Li@ed.ac.uk).

Z. Jiang is with the Robinson Research Institute, Victoria University of Wellington, PO Box 33436, Lower Hutt 5046, New Zealand. (e-mail: zhenan.jiang@vuw.ac.nz).

Y. Xin is with the School of Electrical & Information Engineering, Tianjin University, Tianjin 300072, China. (e-mail: yingxin@tju.edu.cn).

Dynamic loss and resistance are important parameters to evaluate the performance of HTS CCs in power equipment, which is tightly linked to the happening of the quench. They are determined by not only the outer electromagnetic environment, e.g. the applied transport current (I_t) and the external magnetic field (B_{ext}), but also the intrinsic characteristics of the HTS CC, e.g. the critical current in self-field critical current (I_{c0}) and the *n*-value. Although the changing pattern of the dynamic loss/resistance in respect of some external electromagnetic excitation factors has been studied a lot, their variation properties for different types of HTS CCs with distinct I_{c0} and *n*-value are still not clear [11]-[15]. In addition, the functioning mechanism of I_{c0} and *n*-value on the dynamic loss/resistance have not been systematically studied. Therefore, it is necessary to clarify the dependence of dynamic loss and resistance on I_{c0} and *n*-value of HTS CCs.

Based on the validated numerical model in [11], this paper has calculated the dynamic loss and the dynamic resistance with different I_{c0} and *n*-value. During the simulation, the field dependence of the critical current $J_c(B)$ has been taken into account. The simulated results have been validated in comparison with the corresponding experimental measurement data and analytical expressions. The influences of I_{c0} on the $Q_{dyn,n}(I_t)$ curve, the $R_{dyn,n}(I_t)$ curve, the $Q_{dyn,n}(B_{ext})$ curve and the $R_{dyn,n}(B_{ext})$ curve have been studied respectively ($Q_{dyn,n}$ and $R_{dyn,n}$ signify respectively the dynamic loss and the dynamic resistance in unit length during one cycle). Furthermore, the "corner field" B_{cor} has been defined for describing the dynamic loss/resistance in the case where I_t gets superior to $I_c(B_{ext})$. At last, the effect of the *n*-value on the nonlinearity of the dynamic loss/resistance has been specially analyzed.

Through this work, the variation characteristics of the dynamic loss and resistance relating to the critical current in self-field I_{c0} and the *n*-value have been systematically figured out. The results can be used to accurately predicate the dynamic loss and resistance for different types of HTS CCs, and further be a useful reference for loss control.

II. Analysis Method

As shown in Fig. 1, the numerical model of the 1-dimension thin strip was developed by use of the finite element method based on $\boldsymbol{T}$-formulation [16]-[17], in which the current vector potential $\boldsymbol{T}$ on each node is introduced to characterize the current density $\boldsymbol{J}$, $J = \nabla \times T$. The governing equation is derived from Maxwell's equations, as

$$\frac{1}{\sigma}\nabla^2 T - \frac{\mu_0 h}{2\pi}\cdot\frac{\partial}{\partial t}\sum_{en=1}^{e\max}\frac{l_{en}\nabla\times(T_{en}^{e}\boldsymbol{n}')\cdot\hat{\boldsymbol{x}}}{r_{en}} - \frac{\partial \boldsymbol{B}_{ext}}{\partial t}\cdot\boldsymbol{n} = 0 \quad (1)$$

where l_{en} is the width of each element, $\boldsymbol{T}_{en}^{e}$ is the current vector potential in each element, and r_{en} is the distance between the current source element and the calculation point. $\boldsymbol{n}'$ is the normal vector at the current source element, $\boldsymbol{n}$ is the normal vector at the calculation point, and h is the thickness of the HTS layer (neglected compared to the width of mm order level). $\boldsymbol{B}_{ext}$ is the externally applied magnetic field perpendicular to the surface of the conductor, and σ is the equivalent conductivity determined by the E-J power law, with $\sigma = J / E$.

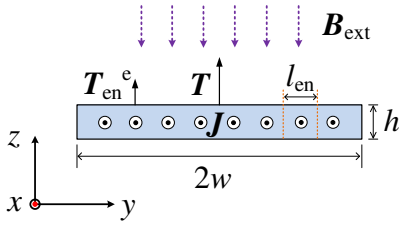

Fig 1. Modeling of the HTS-coated conductor with current density $\boldsymbol{J}$, exposed to external magnetic field $\boldsymbol{B}_{ext}$ perpendicular to its surface, based on $\boldsymbol{T}$-formulation, along its cross section (thickness h, width $2w$).

The magnetic field dependency of the critical current $J_c(B)$ is expressed as

$$J_c(B) = \frac{J_{c0}}{1 + B_{\perp}/B_0} \quad (2)$$

where J_{c0} is the critical current density in self-field, $B_{\perp}$ signifies the total magnetic field component (composed of the self-field and the externally applied field) perpendicular to the surface of the CC, with $B_0 = 0.135$ T, a constant dependent on the material [1, 11]. When a coated conductor carries a DC transport current under an AC magnetic field, the DC current I_t occupies the superconducting layer with width $2iw$ in the center of the coated conductor, leaving the rest with width $(1-i)w$ free on both sides [11]. Therefore, on the basis of (1) and (2), the dynamic during one cycle, Q_{dyn}, can be formulated by

$$Q_{dyn} = \frac{hL}{f}\cdot\int_{(1-i)w}^{(1+i)w} E\cdot J dy = \frac{E_0 hL}{{J_{c0}}^n f}\int_{(1-i)w}^{(1+i)w} J^{n+1}\cdot\left(1+\frac{B_{\perp}}{B_0}\right)^n dy \quad (3)$$

where i is the ratio between the transport current I_t and the critical current in self-field I_{c0}, w is the half width of the HTS-coated conductor, and L is its length. f is the frequency of the AC magnetic field. $E_0 = 10^{-4}$ V/m.

Dynamic loss can also be calculated according to the analytical method in [18]-[19], as the formula

$$Q_{dyn} = I_t\cdot\Delta\Phi = \frac{{I_t}^2\cdot R_{dyn}}{f} = {I_t}^2\cdot\frac{4wL}{I_{c0}}(B_{ext} - B_{th}) \quad (4)$$

where $\Delta\Phi$ is the perpendicular flux crossing the conductor during one cycle, and B_{th} is the threshold field, which is given by [20]

$$B_{th} = B_p\left(1 - \frac{I_t}{I_{c0}}\right) \quad (5)$$

where B_p is the effective penetration field of the CC determined by the B value at the maxima of the Γ curve, with

$$\Gamma = Q_{BI} / {B_{ext}}^2 \quad (6)$$

Q_{BI} is the Brandt expression for magnetisation loss, and

$$Q_{BI} = 4 f w^2 J_{c0} B_{ext}\left[\frac{2B_c}{B_{ext}}\ln\left(\cosh\frac{B_{ext}}{B_c}\right) - \tanh\left(\frac{B_{ext}}{B_c}\right)\right] \quad (7)$$

$$B_c = \frac{\mu_0 J_{c0}}{\pi} \quad (8)$$

where J_{c0} is determined by $I_{c0} / (2wh)$.

Based on (6), (7) and (8), the penetration field can be obtained as

$$B_p = 4.9284\frac{\mu_0 J_{c0} h}{\pi} \quad (9)$$

In this paper, to eliminate the influence of the frequency and better compare the simulation results with the experimental measurements, we define the normalized dynamic loss (J/m) and dynamic resistance (Ω/m/Hz) in unit length per Hz as

$$\begin{cases} Q_{dyn,n} = \dfrac{Q_{dyn}}{L} = {I_t}^2\cdot\dfrac{4w}{I_{c0}}(B_{ext} - B_{th}) \\ R_{dyn,n} = \dfrac{R_{dyn}}{Lf} = \dfrac{4w}{I_{c0}}(B_{ext} - B_{th}) \end{cases} \quad (10)$$

Their derivative with respect to I_{c0} can be obtained as

$$\begin{cases} \dfrac{\partial Q_{dyn,n}}{\partial I_{c0}} = -4w\cdot\dfrac{{I_t}^2}{{I_{c0}}^2}\left(B_{ext} + \dfrac{2.4642\mu_0}{\pi w} I_t\right) \\ \dfrac{\partial R_{dyn,n}}{\partial I_{c0}} = -4w\cdot\dfrac{1}{{I_{c0}}^2}\left(B_{ext} + \dfrac{2.4642\mu_0}{\pi w} I_t\right) \end{cases} \quad (11)$$

III. Dependency of Dynamic Loss and Resistance on Critical Current

The numerical model was established based on the size of an HTS CC manufactured by SuperPower, Inc., which is 4 mm wide comprising a 1-μm thin film of REBCO. A wide range of I_{c0} from 80 A to 160 A was simulated and an external magnetic field was applied perpendicular to the surface of the HTS CC with varying magnitudes. Besides, the experimental measurements mentioned in [11] are referenced here. For the tested HTS CC in the experiment, with $n = 22.5$ and $I_{c0} = 105.3$ A at 77 K, it was exposed to an external magnetic field of 26.62 Hz with a magnitude varying between 0 and 100 mT.

A. *Influence of* I_{c0} on $Q_{dyn,n}(I_t)$

When the amplitude of the externally applied magnetic field B_{ext} is chosen as 40 mT, for different I_{c0}, the dynamic loss curves with respect to I_t are presented in Fig. 2.

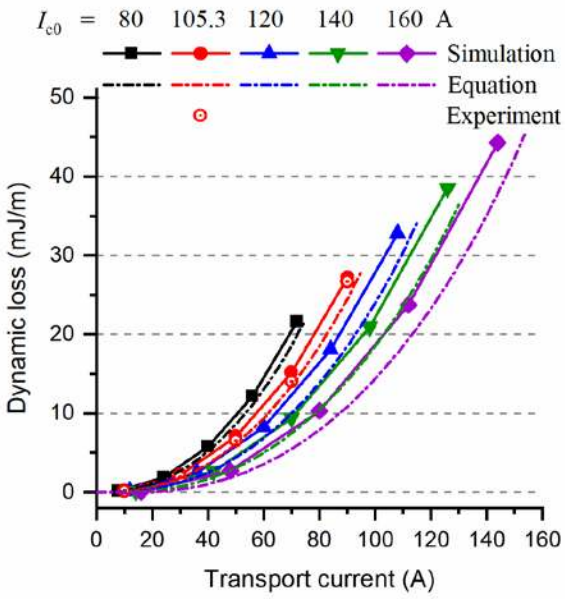

Fig 2. Normalized dynamic loss for different HTS-coated conductors with different I_{c0} when changing transport current, under an AC magnetic field of 40 mT. (I_{c0} = 80 A, 105.3 A, 120 A, 140 A, 160 A, the load rate (I_t / I_{c0}) is set at 10%, 30%, 50%, 70%, and 90%).

In Fig. 2, the solid lines with symbols represent the simulated results, the dash-dot lines signify the analytical results by (10), and the symbols without lines are the experimentally measured results. All these results show good agreement with each other, though the simulated dynamic loss is slightly higher than that of the analytical expression, which is in accordance with [11].It can be found that for the same transport current I_t under the same AC magnetic field, less dynamic loss is generated in the CC with a higher I_{c0}. Taking I_t = 60 A as an example for illustration, when changing I_{c0} from 80 A to 120 A (40 A of augmentation), the normalized dynamic loss varies from 15 mJ/m to 8 mJ/m (reduction of 7 mJ/m). Meanwhile, when I_{c0} is increased from 120 A to 160 A (40 A of augmentation), the dynamic loss drops to 5.8 mJ/m (reduction of 2.2 mJ/m). On this basis, the dynamic loss apparently decreases more slowly with the increase of I_{c0}, which is in good agreement with (11). Therefore, it is not always cost-effective to decrease the dynamic loss simply by increasing I_{c0}.

In fact, the effect of I_{c0} on the dynamic loss is tightly linked to the current load rate I_t / I_{c0}, which can be explained by Fig. 3.

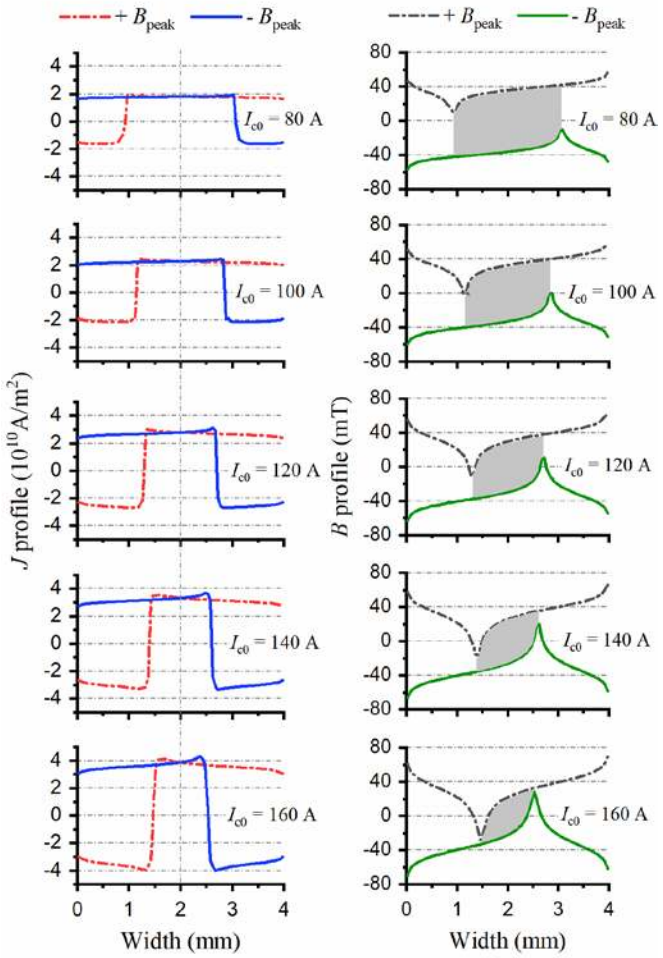

Fig 3. J and B profiles for different HTS-coated conductors with different I_{c0} when carrying the same transport current I_t = 40 A, under an AC magnetic field of 40 mT. (I_{c0} = 80 A, 105.3 A, 120 A, 140 A, 160 A)

Fig. 3 shows the J and B profiles of different HTS CCs with distinct I_{c0} while carrying the same transport current, I_t = 40 A, exposed to an AC magnetic field of which the amplitude B_{ext} = 40 mT. It can be seen that, with the increase of I_{c0}, the J profiles move towards each other and lead to a smaller effective region to carry the transport current. The B profiles have the same trend as the J profiles when I_{c0} gets larger. Here the shaded area signifies the amount of traversing magnetic flux during one AC period, which determines how much dynamic loss is generated. Therefore, with the augment of I_{c0}, the effective region to carry transport current shrinks and then less magnetic flux traverses this region, resulting in less dynamic loss.

B. Influence of I_{c0} on $R_{dyn,n}(I_t)$

Exposed to the same externally applied magnetic field with B_{ext} = 40 mT, for different I_{c0}, the variation characteristics of the dynamic resistance in respect of I_t are presented in Fig. 4. The solid lines with symbols signify the simulation results. In general, the changing trend of the dynamic resistance with respect to I_{c0} follows the same property as the dynamic loss. In other words, for the same transport current I_t, the CC with a higher I_{c0} has a lower dynamic resistance, which complies with (6) and Fig. 3. Again, taking I_t = 60 A as an example, when

changing I_{c0} from 80 A to 120 A, the normalized dynamic resistance varies from 4 $\mu\Omega$/m/Hz to 2.3 $\mu\Omega$/m/Hz (reduction of 1.7 $\mu\Omega$/m/Hz). However, when I_{c0} is increased from 120 A to 160 A, the dynamic resistance decreases to 1.3 $\mu\Omega$/m/Hz (reduction of 1 $\mu\Omega$/m/Hz). Therefore, we can conclude that the dynamic resistance also decreases more slowly with the increase of I_{c0}, which is also in agreement with (11).

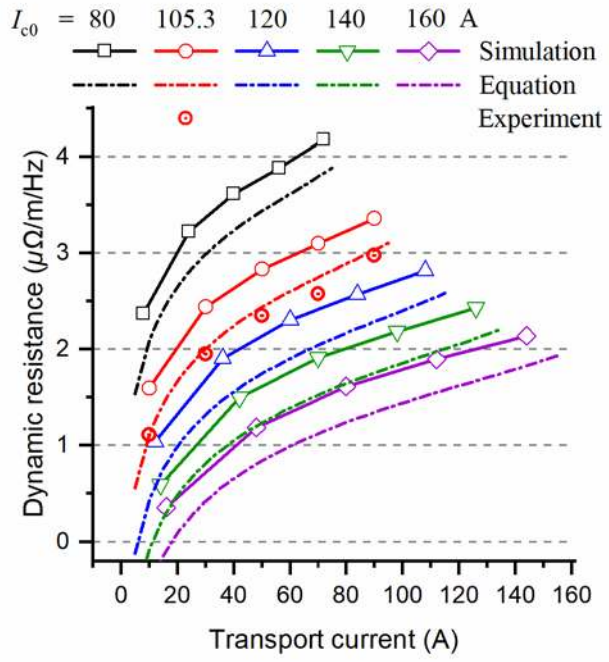

Fig 4. Normalized dynamic resistance for different HTS-coated conductors with different I_{c0} when changing transport current, under an AC magnetic field of 40 mT. (I_{c0} = 80 A, 105.3 A, 120 A, 140 A, 160 A, the load rate is set at 10%, 30%, 50%, 70%, and 90%).

It is also of interest to notify that, $R_{dyn,n}$ increases in a non-linear way with I_t, according to the simulated results. This non-linearity can not be explained by (10). Actually, [12] mentioned that (5) provided good agreement with all previously-published experimental data only for a high load rate (especially for i > 10%). Mikitik and Brandt have proposed another expression for the threshold field [20], as

$$B_{th} = \frac{\mu_0 J_{c0} h}{2\pi}\left[\frac{1}{i}\cdot\ln\left(\frac{1+i}{1-i}\right)+\ln\left(\frac{1-i^2}{4i^2}\right)\right] \quad (12)$$

The nonlinearity of (12) has been verified experimentally in [21]. According to (10) and (12), we have

$$R_{dyn,n} = \frac{4w}{I_{c0}}\cdot B_{ext} - \frac{\mu_0}{\pi}\left[\frac{1}{i}\cdot\ln\left(\frac{1+i}{1-i}\right)+\ln\left(\frac{1-i^2}{4i^2}\right)\right] \quad (13)$$

The calculated dynamic resistance by (13) is depicted in Fig. 4 with dash-dot lines, and the experimental data are plotted with only symbols, both of which agree well with the variation trend of the simulated results. Therefore, it is verified that the dynamic resistance is actually in a non-linear correlation with the transport current.

C. *Influence of* I_{c0} on $Q_{dyn,n}(B_{ext})$ and $R_{dyn,n}(B_{ext})$

When I_{c0} changes from 80 A to 160 A, the variation properties of the normalized dynamic loss $Q_{dyn,n}$ and dynamic resistance $R_{dyn,n}$ relating to the externally applied magnetic field are simulated and compared in Fig. 5. The transport current is chosen as I_t = 40 A, and the amplitude of the applied magnetic field ranges from 0 to 100 mT.

In Fig. 5, among all the $Q_{dyn,n}(B_{ext})$ and $R_{dyn,n}(B_{ext})$ curves, the solid lines with symbols represent the simulated results, the dash-dot lines signify the calculated results by (10), and the symbols without lines are obtained by experiment. It can be found that the simulated results show a good agreement with the analytical expression, while they are in better accordance with the experimental data.

Overall, the dynamic loss and the dynamic resistance show the same trend with the increase of B_{ext}, in that a higher magnetic field can bring more flux that traverses the HTS conductor. Under the same B_{ext}, it can be seen that more dynamic loss and resistance are generated in the HTS CC with a lower I_{c0}. In fact, when carrying the same I_t, a smaller I_{c0} means a higher current load rate. Therefore, in this case, the effective region to carry transport current is larger and more flux will traverse this conductor, then leading to a higher dynamic loss and resistance.

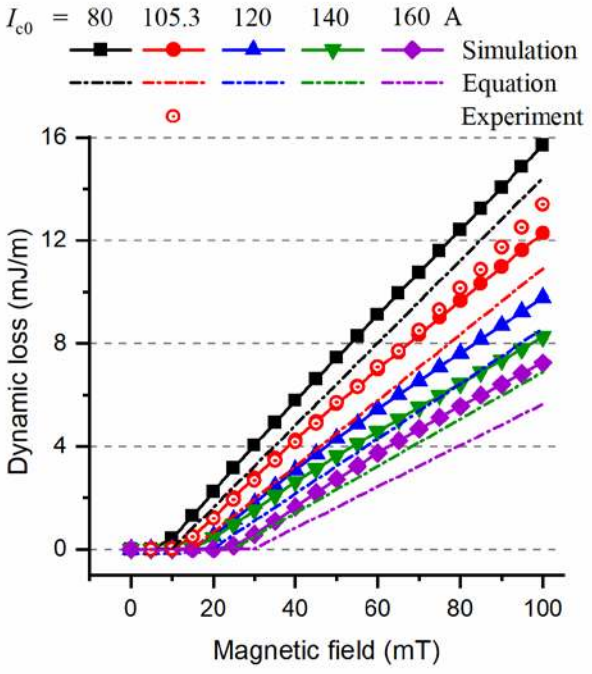

(a)

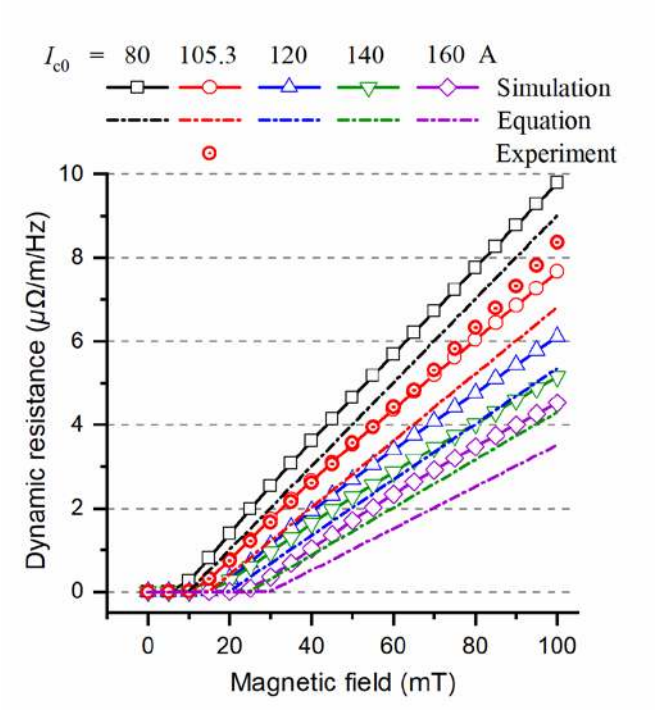

(b)

Fig 5. Normalized dynamic loss and dynamic resistance for different HTS-coated conductors with different I_{c0} when changing externally applied magnetic field from 0 - 100 mT. (I_{c0} = 80 A, 105.3 A, 120 A, 140 A, 160 A, I_t is set as 40 A). (a) Dynamic loss. (b) Dynamic resistance.

Furthermore, the dynamic loss and resistance decrease faster and faster with the increase of I_{c0}. Taking B_{ext} = 60 mT for example, when I_{c0} increases from 80 A to 120 A by 40 A, the normalized dynamic loss drops from 9 mJ/m to 5 mJ/m with a reduction of 4 mJ/m. However, when I_{c0} increases from 120 A to 160 A, the reduction of dynamic loss is only 1.4 mJ/m. Dynamic resistance changes in a similar way. The above conclusions agree well with (11). It is worth mentioning that, only beyond the threshold field B_{th} can the dynamic loss and dynamic resistance be generated, as shown in (5). With the augment of I_{c0}, the critical current density will increase accordingly, which results in a higher B_{th}. The magnetic flux firstly penetrates into the HTS CC from its boundaries to form walls, and then the walls break up into vortices with the increase of B_{ext} [22]. Before that B_{ext} goes beyond B_{th}, the vortices will not diffuse towards the center of the CC, thus no dynamic loss is produced. For the HTS CC with a higher I_{c0}, a greater amount of magnetic flux is needed to penetrate into its interior to form irregular penetrating flux regions, which are the sources of vortex creations.

D. *Influence of* I_{c0} on B_{cor}

On the basis of Fig. 5 (a), when continuing to increase B_{ext}, the $Q_{dyn,n}(B_{ext})$ curves are shown in Fig. 6. The solid lines with symbols represent the simulated results, and the dash-dot lines are obtained by (10). It is of interest to note that, under a high enough B_{ext}, the $Q_{dyn,n}(B_{ext})$ curves show a fast-rising non-linearity, which is distinguished from (10). Here the external magnetic field bringing a sudden change of the dynamic loss is defined as the corner field, B_{cor}. According to (10), the derivative of $Q_{dyn,n}$ (linearly increasing part) with respect to B_{ext} can be written as

$$\frac{\partial Q_{dyn,n}}{\partial B_{ext}} = I_t^2 \cdot \frac{4w}{I_{c0}} \tag{13}$$

B_{cor} is defined when the derivative of $Q_{dyn,n}$ changes by 10%, which clearly differs from linear increase, as (14)

$$\frac{\partial Q_{dyn,n}}{\partial B_{ext}}\Big|_{B_{ext}=B_{cor}} = 1.1 \cdot I_t^2 \cdot \frac{4w}{I_{c0}} \tag{14}$$

Actually, this sudden change appears because of the field dependency of the critical current density $J_c(B)$. With the increase of B_{ext}, the critical current density of the HTS CC will turn lower and its real critical current will be reduced, as a consequence, the load rate will easily go beyond 100% and rapid growth of dissipated power will be generated [11].

At B_{cor}, the real critical current I_{cor} can be approximated as

$$I_{cor} = \frac{I_{c0}}{1 + B_{cor}/B_0} \tag{15}$$

Taking I_{c0} = 80 A in Fig. 6 as an example for illustration, the corner field of its $Q_{dyn,n}(B_{ext})$ curve is around 200 mT, then in this case $I_t / I_{cor\,(200\,mT)}$ = 1.24 > 100%. Therefore, at B_{cor} the real load rate is already superior to 1.

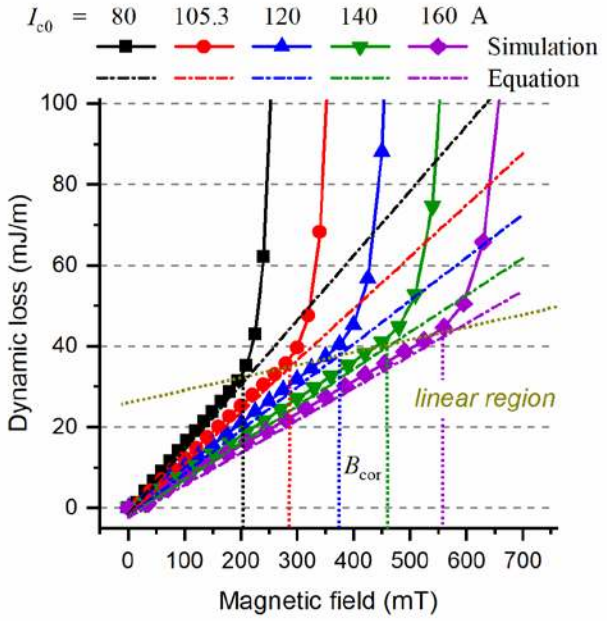

Fig 6. Dynamic loss for different HTS-coated conductors with different I_{c0} when changing externally applied magnetic field from 0 - 500 mT. (I_{c0} = 80 A, 100 A, 120 A, 140 A, 160 A; I_t is set as 60 A). n = 25.

From Fig. 6, it can be found that when increasing I_{c0} from 80 A to 160 A, B_{cor} changes from 80 mT to approximately 300 mT. Actually, when carrying the same transport current, the HTS CC with a higher I_{c0} has a stronger capacity to withstand the current induced by the external magnetic field and it will be harder for the transport current to go beyond the critical current. Therefore, in this case, B_{cor} increases with I_{c0}. In other words, for a high load rate I_t / I_{c0}, the HTS CC is more susceptible to the external magnetic field and its dynamic loss is more likely to have a sudden change under relatively lower B_{ext}.

IV. Dependency of Dynamic Loss on *n*-value

Considering that the $Q_{dyn,n}(B_{ext})$ and $R_{dyn,n}(B_{ext})$ curves have the same variation pattern, thus for this section, only the dynamic loss will be discussed.

Taking the tested HTS CC with I_{c0} = 105.3 A as a prototype for numerical modeling, with the variation of the *n*-value the simulated dynamic losses are presented in Fig.7, as well as the measured results. Fig. 7 (a) shows that for low load rate (e.g. I_t / I_{c0} = 30%), the *n*-value does not have a significant influence on the dynamic loss. However, when the load rate turns high enough (e.g. I_t / I_{c0} = 90%), as shown in Fig. 7 (b), the dynamic loss increases rapidly after reaching B_{cor}. Besides, the larger the *n*-value, the higher the increasing rate, and the lower B_{cor}. In detail, when the *n*-value changes from 20 to 60, B_{cor} decreases from 50 mT to 25 mT. From *n* = 20 to *n* = 40, B_{cor} drops with a difference of 20 mT; however, from *n* = 40 to *n* = 60, B_{cor} drops with a difference of only 5 mT. Therefore, the declining rate of B_{cor} gets smaller with the increase of the *n*-value.

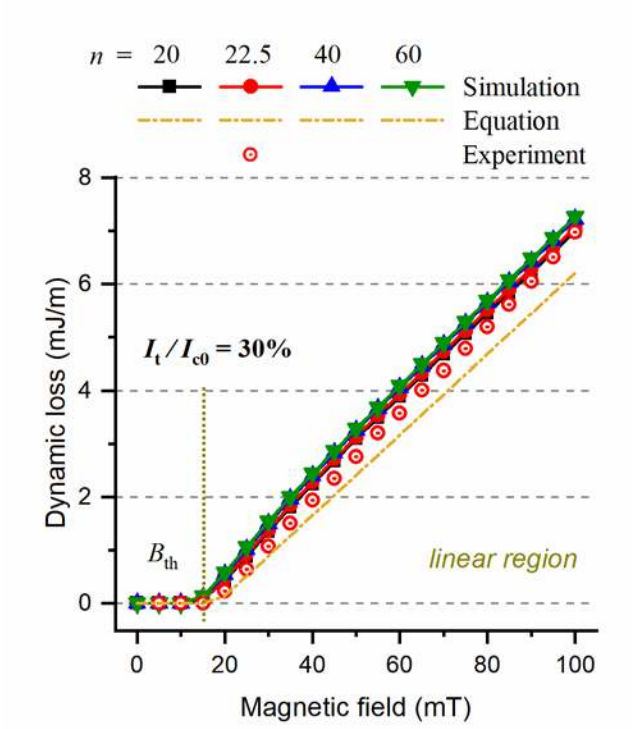

(a)

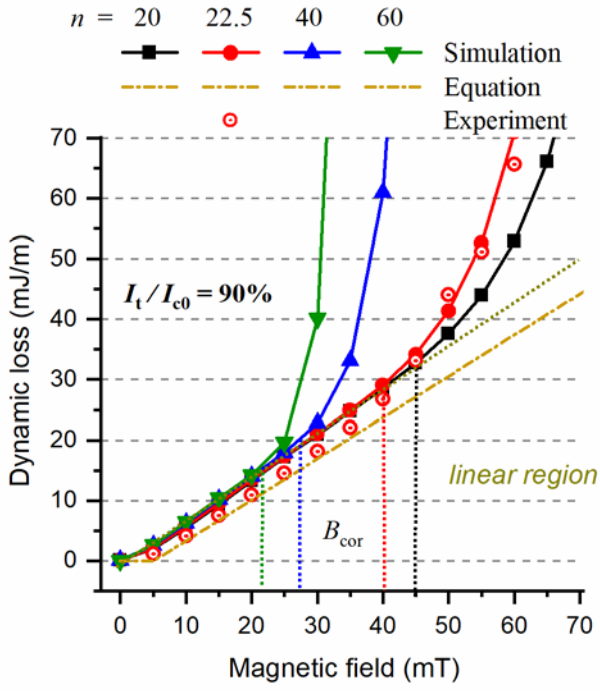

(b)

Fig 7. Dynamic loss for different HTS-coated conductors with different *n*-value when changing externally applied magnetic field from 0 - 100 mT (I_{c0} = 105.3 A). (a) I_t / I_{c0} = 30%. (b) I_t / I_{c0} = 90%.

In fact, according to (3), we know that the dynamic loss is tightly linked to the power function $f(B) = (1+B_\perp/B_0)^n$, caused by the $J_c(B)$ dependency. At low I_t/I_{c0}, and under small B_{ext}, $B_\perp$ is far inferior to B_0. In this way, $f(B)$ approaches to 1, thus the *n*-value does not have a significant impact on the dynamic loss and the $Q_{dyn,n}(B_{ext})$ curve shows linearity. In contrast, at high I_t/I_{c0}, under the influence of B_{ext}, $B_\perp$ will become comparable to B_0. In this case, $f(B)$ will be greatly affected by the *n*-value and after B_{cor} the dynamic loss will increase in the form of the power function. With the augment of the *n*-value, this power function has a higher power index and the dynamic loss will have a higher rate of change. Therefore, the higher the *n*-value, the smaller B_{cor}.

V. Conclusion

This paper has clarified the dependence of the dynamic loss and dynamic resistance on the critical current and the *n*-value of HTS CCs. Based on simulation and experimental results, we found that under the same external electromagnetic environment, dynamic loss and resistance reduces along with increasing I_{c0}. At higher transport current I_t (above 50% I_{c0}), the influence of I_{c0} on dynamic loss and resistance is more obvious, since in principle load rate I_t/I_{c0} directly determines the magnetic flux traversing the HTS conductors.

1) In general, both the dynamic loss and the dynamic resistance increase linearly with the external magnetic field, until it reaches the corner field B_{cor}. When B_{ext} goes beyond B_{cor}, dynamic loss increases in the form of the power function due to the $J_c(B)$ dependence. For a lower

I_{c0} (e.g. load rate above 50%), HTS CCs are more sensible to external magnetic field, and their B_{cor} is lower.

2) n-value is another key property to affect the correlation between dynamic loss/resistance and external magnetic fields. The higher the n-value is, the faster the dynamic loss and resistance increases along with B_{ext}, and the smaller B_{cor} becomes.
3) Dynamic loss and resistance decreases more slowly with the increase of I_{c0}, thus it is not always cost-effective to reduce dynamic loss/resistance by simply increasing I_{c0} during the manufacture of HTS CCs.

It should be emphasized that the nonlinearity of the dynamic loss and the dynamic resistance at high load rate while under high external magnetic field (e.g. I_t /I_{c0} above 90%, B_{ext} above 45 mT, with n = 22.5) cannot be explained and predicted by the existing analytical expressions. Therefore, the numerical modeling method proposed in this paper can more accurately describe the variation properties of the dynamic loss and resistance. Last but not the least, the nonlinearity of the $R_{dyn,n}(I_t)$ curve has been validated experimentally in this paper, which further confirms the correctness of (7).

REFERENCES

[1] M. P. Oomen, *et al*., "Dynamic resistance in a slab-like superconductor with Jc(B) dependence," *Superconductor Science and Technology*, vol. 12, no. 6, pp. 382, 1999.

[2] R. C. Duckworth, *et al*., "Dynamic Resistance of YBCO-Coated Conductors in Applied AC Fields with DC Transport Currents and DC Background Fields," *IEEE Transactions on Applied Superconductivity*, vol. 21, no. 3, pp. 3251-3256, 2011.

[3] Z. Jiang *et al*., "Dynamic Resistance Measurement of a Four-Tape YBCO Stack in a Perpendicular Magnetic Field," *IEEE Transactions on Applied Superconductivity*, vol. 28, no. 4, pp. 1-5, 2018.

[4] Z. Jiang *et al*., "The dynamic resistance of YBCO coated conductor wire: Effect of DC current magnitude and applied field orientation," *Supercond. Sci. Technol.*, 035002, vol. 31, no. 3, 2018..

[5] P. Machura and Q. Li, "A critical review on wireless charging for electric vehicles," *Renewable and Sustainable Energy Reviews*, Vol. 104, pp. 209-234, 2019.

[6] T. Nishimura, T. Nakamura, Q. Li, N. Amemiya and Y. Itoh, "Potential for Torque Density Maximization of HTS Induction/Synchronous Motor by Use of Superconducting Reluctance Torque," *IEEE Transactions on Applied Superconductivity*, vol. 24, no. 3, pp. 1-4, 2014.

[7] Z. Wei, Y. Xin, J. Jin and Q. Li, "Optimized Design of Coils and Iron Cores for a Saturated Iron Core Superconducting Fault Current Limiter," *IEEE Transactions on Applied Superconductivity*, vol. 26, no. 7, pp. 1-4, 2016.

[8] Q. Li, N. Amemiya, K.Takeuchi, *et al*., "Effects of unevenly distributed critical currents and damaged coated conductors to AC losses of superconducting power transmission cables," *IEEE Transactions on Applied Superconductivity*, vol. 21, no. 3, pp. 953-6, 2011.

[9] Q. Li, N. Amemiya, R. Nishino, *et al*., "AC loss reduction of outer-diameter-fixed superconducting power transmission cables using narrow coated conductors, " *Physica C Superconductivity*, vol. 484, no. 1, pp. 217-222, 2013.

[10] Z. Wei, Y. Xin, W. Hong, *et al*., "A new type of DC superconducting fault current limiter," *IEEE Transactions on Applied Superconductivity*, vol. 29, no. 5, 5602905, 2019.

[11] Q. Li, M. Yao, Z. Jiang, C. W. Bumby and N. Amemiya, "Numerical Modeling of Dynamic Loss in HTS-Coated Conductors Under Perpendicular Magnetic Fields," *IEEE Transactions on Applied Superconductivity*, vol. 28, no. 2, pp. 1-6, 2018.

[12] Y. Liu, Z. Jiang, Q. Li, C. W. Bumby, R. Badcock and J. Fang, "Dynamic resistance measurement in a four-tape YBCO stack with various applied field orientation," *IEEE Transactions on Applied Superconductivity*, 2019. (Early Access)

[13] Z. Jiang, R. Toyomoto, N. Amemiya, C. W. Bumby, R. A. Badcock and N. J. Long, "Dynamic Resistance Measurements in a GdBCO-Coated Conductor," *IEEE Transactions on Applied Superconductivity*, vol. 27, no. 4, pp. 1-5, 2017.

[14] R. C. Duckworth, Y. F. Zhang, T. Ha and M. J. Gouge, "Dynamic Resistance of YBCO-Coated Conductors in Applied AC Fields With DC Transport Currents and DC Background Fields," *IEEE Transactions on Applied Superconductivity*, vol. 21, no. 3, pp. 3251-3256, 2011.

[15] K. Hattori *et al*., "Estimation of Dynamic Resistance Variations in YBCO Thin Film for Optimization Design of Superconducting Fault Current Limiter," *IEEE Transactions on Applied Superconductivity*, vol. 23, no. 3, pp. 5602005-5602005, 2013.

[16] Q. Li, N. Amemiya, K. Takeuchi, et al, "AC loss characteristics of superconducting power transmission cables: gap effect and Jc distribution effect," *Supercond. Sci. Technol.*, 115003, vol. 23, no. 11, 2010.

[17] Q. Li, H. Tan and X. Yu, "Effect of multilayer configuration on AC losses of superconducting power transmission cables consists of narrow coated conductors," *IEEE Transactions on Applied Superconductivity*, 5400604, vol. 24, no. 5, 2014.

[18] T. Matsushita, *Flux Pinning and Electromagnetic Phenomenon*. Tokyo, Japan: Sangyo Tosho, Inc., pp.99, 1994.

[19] Z. Jiang, *et al*., "Dynamic resistance of a high-Tc superconducting flux pump." *Applied Physics Letters*, vol. 105, no. 11, 2014:3600104.

[20] G. P. Mikitik and E. H. Brandt, "Generation of a dc voltage by an ac magnetic field in type-II superconductors," *Physical Review B*, vol. 64, no. 9, 2001:092502.

[21] Z. Jiang, *et al*, "Dynamic resistance of a high-Tc coated conductor wire in a perpendicular magnetic field at 77 K ", *Supercond. Sci. Technol.*, vol. 30, no. 3, 2017.

[22] Y. Enomoto, *et al*, "Simulation study on the first penetration field in type-II superconductors", *Journal of Physics: Condensed Matter*, vol. 9, pp. 10203-10209, 1997.